Earth and Planetary Science Letters 430 (2015) 486–498

Contents lists available at ScienceDirect

Earth and Planetary Science Letters

www.elsevier.com/locate/epsl

The solubility of rocks in metamorphic fluids: A model for rock-dominated conditions to upper mantle pressure and temperature

Matthieu E. Galvez [a,b,*], Craig E. Manning [c], James A.D. Connolly [b], Douglas Rumble [a]

[a] Geophysical Laboratory, Carnegie Institution for Science, 5251 Broad Branch Road NW, Washington, DC 20015, USA
[b] Department of Earth Sciences (Institute of Geochemistry and Petrology), Swiss Federal Institute of Technology, CH-8092 Zurich, Switzerland
[c] Department of Earth, Planetary & Space Sciences, University of California, Los Angeles, CA, USA

ARTICLE INFO

Article history:
Received 8 October 2014
Received in revised form 9 June 2015
Accepted 11 June 2015
Available online 25 August 2015
Editor: B. Marty

Keywords:
metasomatism
phase equilibria modeling
COH solutions
dielectrics
polymerization
*p*H

ABSTRACT

Fluids exert a key control on the mobility of elements at high pressure and temperature in the crust and mantle. However, the prediction of fluid composition and speciation in compositionally complex fluid–rock systems, typically present in subduction zones, has been hampered by multiple challenges. We develop a computational framework to study the role of phase equilibria and complex solid-solutions on aqueous fluid speciation in equilibrium with rocks to 900 °C and 3 GPa. This is accomplished by merging conventional phase-equilibrium modeling involving electrolyte-free molecular fluids, with an electrostatic approach to model solute–solute and solute–solvent interactions in the fluid phase. This framework is applied to constrain the activity ratios, composition of aqueous solutes, and *p*H of a fluid in equilibrium with a pelite lithology. Two solvent compositions are considered: pure H_2O, and a COH fluid generated by equilibration of H_2O and graphite. In both cases, we find that the *p*H is alkaline. Disparities between the predicted peralkalinity of our fluid ([Na] + [K])/[Al] ∼ 6 to 12 and results from independent mineral solubility experiments (∼2) point to the presence of Na–K–Al–Si polymers representing *ca.* 60 to 85% of the total K and Al content of the fluid at 600 °C and 2.2 GPa, and to an important fraction of dissolved Ca and Mg not accounted for in present speciation models. The addition of graphite to the system reduces the relative permittivity by *ca.* 40% at elevated *T* and low *P*, triggers the formation of C-bearing anions, and brings the *p*H closer to neutrality by up to 0.6 units at low *T*. This ionic C pool represents up to 45 mol% of the fluid ligands at elevated *P*, and is dominant at low *P* despite the low ionic strength of the fluid (<0.05). The present study offers new possibilities for exploring redox–*p*H dependent processes that govern volatile, major and trace element partitioning between rocks and fluids in experimental or natural systems.

1. Introduction

Metamorphic fluids exert a major control on rheology, reaction kinetics and the transport of heat and matter in the crust and mantle (*e.g.*, Fyfe et al., 1978). Water, in particular, is a powerful solvent for transporting mass on and inside the Earth (*e.g.*, Walther and Helgeson, 1980; Manning, 1994; Ague, 1994; Mottl et al., 2004), participating in its long term differentiation. However, metamorphic fluids commonly contain a range of C-bearing species, characterized by no or low permanent dipole moment, that weaken their solvent property (*e.g.*, Deul and Franck, 1991; Walther and Schott, 1988; Walther, 1992). Nevertheless, fluids rich in molecules such as CO_2, CH_4 and/or N_2 also contain dissolved solutes, *e.g.* Na^+, K^+, Cl^-, that may precipitate as daughter minerals in fluid inclusions upon decompression and cooling (*e.g.*, Andersen et al., 1989; Philippot and Selverstone, 1991; Frezzotti et al., 2011; Ague and Nicolescu, 2014). Moreover, specific patterns of element gain-loss or isotopic systematics provide indirect geochemical evidences for COH fluid-mediated mass transfer, despite their less favorable solvent properties, in a wide range of metamorphic settings (*e.g.*, Bebout and Barton, 1993; Penniston-Dorland and Ferry, 2008; Malvoisin et al., 2012; Galvez et al., 2013a, 2013b; Ague and Nicolescu, 2014).

Despite their importance as metasomatic agents, little is known about dissolution mechanisms, and electrolyte transport in COH fluids (*e.g.*, Evans et al., 2009; Schmidt, 2014). Quantitative prediction of solute mobilization and transport by COH fluids hinges on accurate knowledge of the thermodynamic properties of solvents, solutes, minerals and their solution properties over a wide range of pressure (*P*) and temperature (*T*) conditions. Predic-

* Corresponding author at: Department of Earth Sciences (Institute of Geochemistry and Petrology), Swiss Federal Institute of Technology, CH-8092 Zurich, Switzerland.
E-mail addresses: matthieu.galvez@erdw.ethz.ch, matthieu.galvez@gmail.com (M.E. Galvez).

http://dx.doi.org/10.1016/j.epsl.2015.06.019
0012-821X/

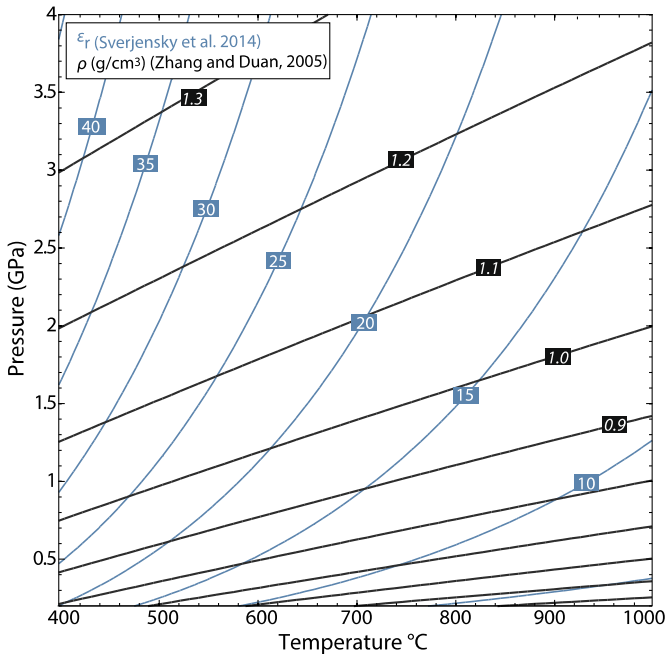

Fig. 1. Contour plot of the static relative permittivity of H_2O $(\varepsilon_r)_{H_2O}$ (EoS developed by Sverjensky et al., 2014) along with density values from Zhang and Duan (2005). There is an increase of $(\varepsilon_r)_{H_2O}$ with density increase along isotherms, and with temperature decrease along isochores over the P–T conditions of interest. This can be explained by a combination of bulk and microstructural factors (*e.g.*, Kirkwood, 1939; Yoshii et al., 2001): With increasing temperature along isochores, higher kinetic energies of water molecules induce partial breakage of the hydrogen bond network between water dipoles, progressively annihilating the intermolecular orientational correlation contribution to the overall polarization (for relatively constant dipole moment of individual molecules) and, induce a drop in $(\varepsilon_r)_{H_2O}$. With isothermal density increase the tight packing of water molecules and increased hydrogen bonding of H_2O invariably favors an increase of $(\varepsilon_r)_{H_2O}$ (*cf.* Appendix A). (For interpretation of the references to color in the figure legends of this paper, the reader is referred to the web version of this article.)

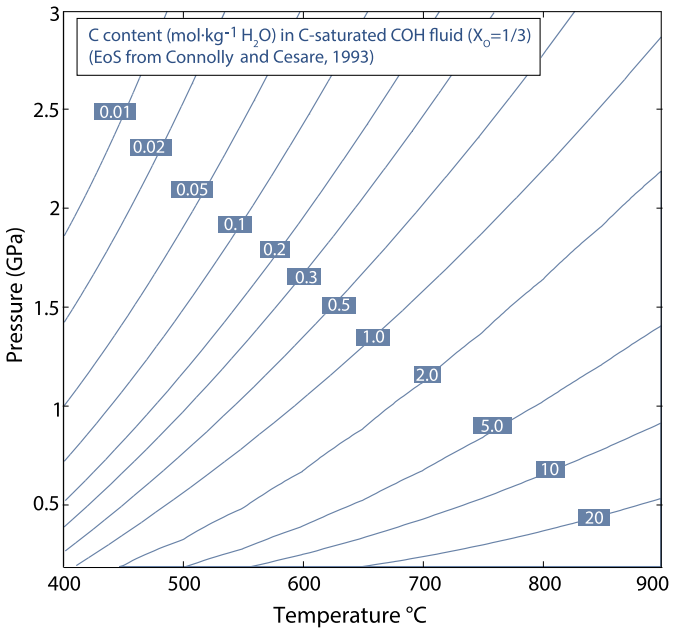

Fig. 2. Contour plot of C molality (mol·kg^{-1} H_2O) in a C-saturated (graphite) COH fluid at $X_O = 1/3$. The EoS used is from Connolly and Cesare (1993), and it assumes that the solid C phase is perfectly crystalline graphite, refer to Appendix B for details. The C molality spans a large range (10^{-3} to >10 molal) and reaches the highest values at elevated T and lower P as can be expected from the weakly polar nature of H_2O at these conditions, *i.e.* where $(\varepsilon_r)_{H_2O}$ is lowest (Fig. 1). The log $f(O_2)$ of this fluid ranges between −2.5 (elevated T and low P) and 0 log units (elevated P and low T) below the fayalite–magnetite–quartz (FMQ) equilibrium log $f(O_2)$. Interestingly, the solubility of $CaCO_3$ in pure H_2O (Caciagli and Manning, 2003) displays comparatively limited variations around 0.01 to 0.3 molal in this P–T range, and only equals or exceeds that of C at the high P and low T conditions typical of the blueschist–lawsonite facies (*cf.* Fig. 4) where $(\varepsilon_r)_{H_2O}$ is highest (Fig. 1). This geochemical feature is noteworthy given the dramatically different structure, properties and kinetics of dissolution of these important C-bearing minerals.

tion of how rock-forming chemical components are redistributed between mineral and fluids has depended chiefly on independent models of the thermodynamic properties of aqueous electrolytes (*e.g.*, Helgeson and Kirkham, 1976; Helgeson et al., 1981; Wolery, 1992) and have been hampered by two main challenges. The first challenge is that there have been limitations to assessing the solvent properties of H_2O beyond the P–T range of the commonly used Helgeson–Kirkham–Flowers (HKF) equations of state: In this model, the partial molal Gibbs free energy of hydration ΔG_{solv} of an ion in a solvent follows the Born equation (Helgeson et al., 1981):

$$\Delta G_{solv,j} = \omega_j \left(\frac{1}{\varepsilon_r} - 1 \right) \tag{1}$$

where ε_r is the relative permittivity of the solvent at P and T, and ω_j is the absolute Born coefficient of the species j. The Born coefficient is an ion-specific function of the ionic charge Z_j, of the effective electrostatic radius (a function of P and T, see Appendix B), and of the vacuum permittivity. The conventional Born coefficient used is defined as $\overline{\omega}_j = \omega_j - |Z_j|\omega_{H^+}$. Expressions for the relative permittivity of pure water, $(\varepsilon_r)_{H_2O}$, as a function of density and temperature were long restricted to <0.5 GPa (*e.g.*, Archer and Wang, 1990). However, quantification of $(\varepsilon_r)_{H_2O}$ has now been extended to *ca.* 6 GPa, and *ca.* 1000 °C (Fernandez et al., 1997; Pan et al., 2013; Sverjensky et al., 2014, and Fig. 1). Building on these fundamental advances, this paper explores the new opportunity for integrating petrologic models of rock systems with models of electrolyte chemistry to high P and T.

The second challenge is that there have also been limitations in the extension of the HKF model to geologically complex solvents that contain, in addition to H_2O, species such as CO_2 and CH_4 (*e.g.*, Connolly and Cesare, 1993). C concentrations may reach tens of molal in such fluids at elevated T and P and $X_O = 1/3$ (Fig. 2) ($X_O = n_O/(n_O + n_H)$), and the molar fraction of carbon-bearing species may even exceed that of H_2O during metamorphism of some carbonate lithologies. In such mixed-volatile mixtures, the density and solvent properties, *e.g.* $(\varepsilon_r)_{mix}$, deviate from those of pure H_2O (Fig. 1). Although changes to the ion-solvation energetics (Eq. (1)) can nominally be derived using predictions of the relative permittivity of mixtures between molecules of geological interest (*e.g.*, Looyenga, 1965; Kirkwood, 1939; Wang and Anderko, 2001), this has only rarely been attempted for metamorphic fluids, and, to our knowledge, only to 0.5 GPa (*e.g.*, Walther, 1992; Evans et al., 2006). These two challenges have prevented the application of the HKF model to fluid speciation at lower-crustal and subduction-zone conditions.

An alternative approach to fluid speciation exploits the empirical observations of log–log linear relationships between the dissociation constants of aqueous complex, $(\varepsilon_r)_{H_2O}$, and ρ_{H_2O} at elevated P and T (*e.g.*, Marshall and Franck, 1981; Manning, 1998; Dolejš and Manning, 2010; Dolejš, 2013) to alleviate the need for values of $(\varepsilon_r)_{H_2O}$ beyond its range of calibration. However, this method remains largely empirical and does not provide insight into key solvent and solute properties. Moreover, this approach is cumbersome to include with accurate, comprehensive description of the changing compositions of complex mineral solid-solutions that occur in realistic petrological systems over the wide range of P and T relevant to metamorphism, which may include shallow magma-hydrothermal systems, orogenic belts or subduction zones. In contrast, while petrological modeling generally account for com-

plex solid solution behavior, such models routinely neglect solutes in the coexisting fluid phase.

In the present study, we develop a method that provides insight into the composition and speciation of high-pressure mixed-solvent fluids at equilibrium with assemblages of complex mineral solid solutions. We present the formal basis for this approach which combines, through general hydrolysis equilibria, the Gibbs free energy of oxide components retrieved from phase equilibrium modeling of solids and molecular fluids, with the Gibbs free energy of dissolved solutes. The latter are derived by an extension of classical electrostatic modeling of COH solution chemistry to extreme P and T, and further constrained by charge balance. The utility of the approach is illustrated using a model metapelite rock at 400–900 °C and 0.2–3.0 GPa, with and without graphite. Our model provisions for the change in ion-solvation energetics by computing the relative permittivity of a COH fluid at $X_O = 1/3$, a reasonable model for a fluid generated by metapelite devolatilization. This approach is designed to isolate and investigate how constituent minerals control the composition and speciation of fluids associated with the rock they form. The results produced are compared with independent experimental data on similar bulk system, and offer a unique window into elusive processes of ionic association at elevated P and T. The outcome is a computational framework within which to investigate the role of metamorphic phase equilibria and complex solid-solutions on the speciation of C-bearing fluids with changing solvent properties to elevated P and T.

2. Computational approach

2.1. Background

The composition of petrological systems can be described by a set of chemical components representing relevant rock- and fluid-forming constituents. For most natural rocks, up to 12 oxide components are adequate to model phase equilibria over a wide range of P and T. The dissolution of rock-forming minerals in aqueous fluids can be represented, in terms of an oxide M_xO_y, by the general hydrolysis reaction:

$$M_xO_y + 2yH^+ = xM^{2y/x+} + yH_2O. \tag{2}$$

At equilibrium, the chemical potentials (μ) of the oxide components are linked to the partial molar Gibbs free energy ($\bar{g}$) of their corresponding dissociated species, here $M^{2y/x+}$, through:

$$\mu(M_xO_y) + 2y \cdot \bar{g}(H^+) = x \cdot \bar{g}(M^{2y/x+}) + y \cdot \mu(H_2O) \tag{3}$$

Equations (2) and (3) make it possible to bring together the two traditional forms of thermodynamic modeling of fluid–rock interaction because they quantitatively relate the chemical potentials of metal oxides, electrolytes and H_2O (Helgeson, 1968). Using oxides in Eqs. (2) and (3) is a particularly convenient way to account for changing mineral solid-solutions over a wide range of P and T in our model. At a given P and T, the chemical potentials of oxide components are obtained by Gibbs energy minimization of a system composed of minerals and of a molecular fluid. The values of μ derived from this model are then employed for purposes of computing the solute speciation. This is valid for closed, rock-dominated system provided the chemical potential retrieved by Gibbs energy minimization (metal oxides and volatile solvent components) are insensitive to the amount of solute in the fluid, which is the case here. Accordingly, the chemical potential of the i^{th} oxide component is the partial derivative of the Gibbs free energy of the solute-free system (G^{sys}) with respect to its number of moles n_i:

$$\mu_i = \left(\partial G^{sys}/\partial n_i\right)_{T,P,n_k} \tag{4}$$

Table 1
Frequently used symbols.

μ_i	the chemical potential of the i^{th} component
$\bar{g}_j$	the partial molar Gibbs free energy of the j^{th} aqueous species
$\bar{g}^\circ_j$	the standard partial molal Gibbs free energy of the j^{th} aqueous species
$(\rho_m)_i$	the molar density of the i^{th} component
P_i	the polarization of the i^{th} component
$(\varepsilon_r)_i$	the (static) relative permittivity of the i^{th} component: $\varepsilon_r = \frac{\varepsilon}{\varepsilon_0}$ with ε_0 the vacuum permittivity, ε the absolute permittivity
$V_{m,i}$	the molar volume of the i^{th} component
$V_{f,i}$	the volume fraction of the i^{th} component
v^*_i	the critical volume of the i^{th} component
x_i	molar fraction of the i^{th} component
$\gamma_{D,j}$	the activity coefficient (long range ionic interactions) of monovalent ($j=1$) or divalent ($j=2$) species
a_i	the activity of the i^{th} component
Ξ^i_j	the log 10 of the ratio among activities of cation i over activity of cation j

and for the j^{th} ion, or neutral complex,

$$\bar{g}_j = \bar{g}^\circ_j + RT \ln a_j \tag{5}$$

where $\bar{g}^\circ_j$ and a_j are, respectively, the standard partial molal Gibbs free energy and activity of the j^{th} solute at P and T (*cf.* frequently used symbols in Table 1). For aqueous species, we adopt the conventional thermodynamic property $\bar{\omega}_{H^+} = 0$ leading to $\bar{g}^\circ(H^+) = 0$ (Eq. (1)). It follows that

$$\ln\left[\frac{a(M^{2y/x+})}{a(H^+)^{2y/x}}\right] = \frac{1}{RT}\left[\mu(M_xO_y) - y \cdot \mu(H_2O)/x - \bar{g}^\circ\left(M^{2y/x+}\right)\right] \tag{6}$$

Equation (6) indicates that the ion activity ratio can be derived from the chemical potentials of an appropriate combination of the system's components if $\bar{g}^\circ_j$ at P and T can be determined consistently at a given P and T (Appendix B). Note that for the other species in solution such as hydroxides (*e.g.*, $CaOH^+$, $MgOH^+$ or AlO_2^-), the form of equation (6) is slightly modified with no change in the underlying principle.

In Eq. (6) we use ion activity ratios because, historically, they have been widely used for the depiction of mineral–fluid equilibria (*e.g.*, Bowers et al., 1984). For more compact notation, we define Ξ^b_a as the logarithm in base 10 of the activity ratio of ions a and b. For example, for Eq. (2),

$$\Xi^{M^{2y/x+}}_{H^+} \equiv \log\left[\frac{a(M^{2y/x+})}{a(H^+)^{2y/x}}\right] \tag{7}$$

The standard state for H_2O is taken to be unit activity of the pure phase at any P and T, and for electrolytes it is unit activity of the hypothetical solution of 1 mole of solute in 1000 g of H_2O, referenced to infinite dilution. The $\bar{g}^\circ$ for ions in pure H_2O can be determined using the HKF equations of state (Helgeson et al., 1981) as revised and extended by Tanger and Helgeson (1988) and Shock et al. (1992). Here, $(\varepsilon_r)_{H_2O}$ is computed at P and T with an EoS from Sverjensky et al. (2014) with input H_2O densities from Zhang and Duan (2005) (Fig. 1), and the thermochemical data for aqueous species are those compiled and revised by Sverjensky et al. (2014) unless otherwise stated (*cf.* Appendix B). Various methods have been developed to assess the role of mixed-solvent on fluid speciation: Walther and Helgeson (1980) advocated explicit provision for ionic hydration to rigorously capture the effect of reduced water activity on solute activity, although the method remained qualitative to a large extent (*cf.* Bowers et al., 1984). Alternatively,

the ion solvation energetics can be quantified by adjusting the solvation term of the Gibbs free energy of ions (Eq. (1)) in order to account for changes of dielectric property of the mixed solvent (Dandurand and Schott, 1992; Walther, 1992). We adopt the second option, which requires computing the relative permittivity of mixed volatile solvents $(\varepsilon_r)_{mix}$.

2.2. Relative permittivity of COH fluid

Diluting H_2O by addition of molecular COH species modifies the bulk properties of the solvent, including $(\varepsilon_r)_{mix}$ (*e.g.*, Looyenga, 1965; Harvey and Prausnitz, 1987; Walther, 1992). To quantify this effect, the molar fraction of the species that dominate the COH speciation at these elevated T and P, *i.e.* H_2O, CO_2 and CH_4, are computed with an EoS from Connolly and Cesare (1993). Despite limitations of this molecular model in providing the exact speciation at elevated P (>2 GPa) and low T (<500 °C) where non-ideality increases rapidly (*e.g.*, Aranovich and Newton, 1999) and solutions are very dilute (Fig. 2), these were considered irrelevant for the present purpose of the study.

To compute $(\varepsilon_r)_{mix}$ for COH molecular mixtures, one option is to employ mixing rules based on the additivity of the cube roots of the relative permittivity of intermixing species (Landau and Lifshitz, 1960; Looyenga, 1965). This approach has received considerable interest in the geologic community as a means of explaining high T mineral solubility data (*e.g.*, Walther, 1992), by virtue of its success at predicting the dielectric properties of supercritical mixtures of polar and non-polar species (*e.g.*, Deul and Franck, 1991). However, this method was initially derived under the assumption that the relative permittivity of intermixing species are similar (*e.g.* Looyenga, 1965). As an alternative, we extend to geologic fluids a mixing scheme developed by Harvey and Prausnitz (1987) which has no theoretical restrictions as to the nature and properties of intermixing species, derives $(\varepsilon_r)_{mix}$ from estimates of the polarization per unit volume (P_{mix}) of the mixture as originally proposed [*e.g.* Eq. (16) in Kirkwood, 1939], and is applicable to non-ideal systems with excess volume of mixing. In this model, $(\varepsilon_r)_{mix}$ is given by:

$$(\varepsilon_r)_{mix} = \frac{1}{4}\left(1 + 9\mathrm{P}_{mix} + 3\left[9\mathrm{P}_{mix}^{2} + 2\mathrm{P}_{mix} + 1\right]^{\frac{1}{2}}\right) \tag{8}$$

where P_{mix} is obtained by linear combination of the contribution of each i^{th} component ($V_{f,i}\mathrm{P}_i$) to the polarization of the mixture (*e.g.*, Kirkwood, 1939), $\mathrm{P}_{mix} = \sum_i V_{f,i}\mathrm{P}_i$, and $V_{f,i}$ is the volume fraction of species i in the mixture at P and T of interest. The computation of $V_{f,i}$ uses a method described in Harvey and Prausnitz (1987) and is outlined in Appendix A. The P_i are functions of the species molar density $(\rho_m)_i$ (reciprocal of their molar volume) and of the temperature calibrated to liquid-like densities by Harvey and Lemmon (2005). The polarization of H_2O at P and T is computed using Eq. (8) (Kirkwood, 1939) with input values for $(\varepsilon_r)_{H_2O}$ from Sverjensky et al. (2014) where H_2O density is from Zhang and Duan (2005). The values of (ρ_m) for CH_4 and CO_2 in the non-ideal mixture are scaled back to the P and T of interest using the relation $(\rho_m)_i = \kappa/v_i^*$, where v_i^* is the critical volume of species i and κ is the critical density of the COH fluid at the P and T of interest computed using an EoS from Connolly and Cesare (1993). It is apparent that the linearity of such mixing scheme requires that the values of P_i of pure components are unchanged upon mixing of polar and non-polar species. Consequently, this model does not account for the experimental evidences showing the fragmentation of the H-bond network of water by addition of non-polar solutes (*e.g.*, Dubessy et al., 1999; Botti et al., 2008) and it can be anticipated that this approach should slightly overestimate $(\varepsilon_r)_{mix}$, although experimental validations are needed. This hypothesis is currently being tested by way of molecular dynamics (MD) simulations of $(\varepsilon_r)_{mix}$ in the binary H_2O–CO_2 system to 725 °C and 3 GPa (Mountain and Harvey, submitted). The values of $(\varepsilon_r)_{mix}$ obtained with an alternative method to estimate the volume fractions (*i.e.* by computing the partial molar volumes of each species at the P–T of interest) and with another mixing rule (Landau and Lifshitz, 1960; Looyenga, 1965, Appendix A) indicate that uncertainties on $(\varepsilon_r)_{mix}$ are everywhere within *ca.* 2–5% in the sub-solidus region (and <16% in the entire P–T range). As a consequence, the anticipated errors on $\bar{g}_j^{\circ}$ (<3000 J/mol at subsolidus conditions) or on equilibrium constants do not impact the results obtained in this study (Appendix A).

The variation of $(\varepsilon_r)_{mix}$ shown in Fig. 3a, c mostly reflects the increasing molar fraction of non-polar C-bearing species in the COH fluid at elevated P and T (Fig. 2). For example, at $P = 1$ GPa and $T = 700$ °C, where the concentration of C in C-saturated COH fluid at $X_O = 1/3$ is *ca.* 2 molal, $(\varepsilon_r)_{mix}/(\varepsilon_r)_{H_2O} \sim 0.9$. The values of $(\varepsilon_r)_{mix}$ are used to compute $\bar{g}^{\circ}$ in Eq. (6) from Eq. (1). That is, the energetics of ions in going from a pure H_2O fluid to a COH mixture, *i.e.* the dielectric correction to the solvation term, Eq. (1) (Appendix B), is incorporated to the standard state Gibbs free energy of the ions in the mixed-solvent. Accordingly, the modified standard state corresponds to unit activity of the solution of 1 mol of solute in 1000 g of the mixed solvent composed of uncharged COH molecular species and referenced to infinite dilution. As a result, the activity coefficients of ions only include non-ideality arising from long range ionic interaction (Helgeson et al., 1981), and are described below by the Davies equation (other details of the computational strategy and conventions are outlined in Appendix B). The values of $(\varepsilon_r)_{mix}$ can be used, in particular, to show how the values of $p\mathrm{H}$ at acid–base neutrality in the mixture ($p\mathrm{H}_w^{mix}$) – *i.e.* $a(\mathrm{H}^+) = a(\mathrm{OH}^-)$ – increase in response to the presence of additional COH molecular species (Fig. 3b).

3. Applications to a model subaluminous pelite system

3.1. Description of the models and main assumptions

We consider two models involving minerals in the Na_2O–CaO–K_2O–FeO–MgO–Al_2O_3–SiO_2–O–H±C system, in which a fluid is equilibrated with an average sub-aluminous pelite, with slightly reduced CaO content (*e.g.*, Caddick and Thompson, 2008). The ubiquity of graphitic material in pelitic rocks makes it a particularly useful lithology to evaluate the role of C on fluid speciation at depth. Model #1 is carbon free and assumes that the fluid is pure H_2O. Model #2 is carbon bearing and assumes a C-saturated COH fluid with $X_O = 1/3$ (and the molecular species H_2O, CO_2, CO, CH_4, H_2 and O_2; Connolly and Cesare, 1993). Equilibrium phase relations are computed at 400–900 °C and 0.2–3.0 GPa. The fluid phase is considered to be present in excess over the entire P–T range. The bulk rock composition is constant except for H_2O, which varies with the change in phase assemblage as required by the assumption of fluid saturation. Melting was not considered in these computations which use end-member thermodynamic data from Holland and Powell (1998, 2002 revision). Mineral solid solution models are listed in Appendix C.

The P–T section for the metapelite bulk composition is shown in Fig. 4. The position of the H_2O-saturated solidus is also indicated (model #1) to highlight the P–T domain where the calculations are metastable with respect to a silicate liquid in model #1 (*cf.* Appendix C). The solidus would be at a marginally higher T at any P in the presence of a COH fluid (model #2). No carbonate minerals are predicted to be stable at any of the P–T conditions investigated (see also Fig. 2). The bulk H_2O content is illustrated using the contours of water weight fraction in the rock at equilibrium

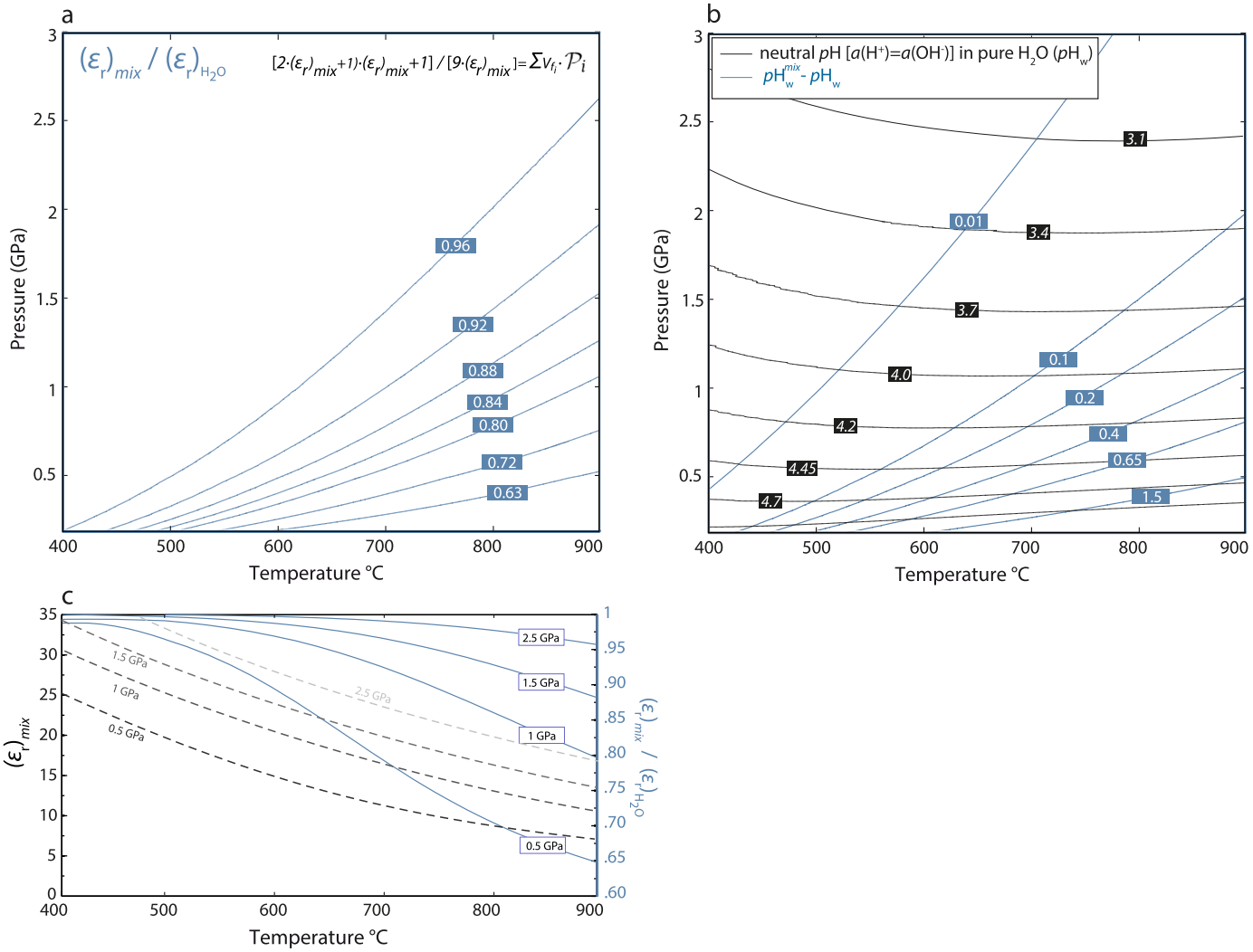

Fig. 3. a. Ratio of the relative permittivity of a COH fluid $(\varepsilon_r)_{mix}$ to that of pure H_2O $(\varepsilon_r)_{H_2O}$. $(\varepsilon_r)_{mix}$ has been estimated using the EoS from Connolly and Cesare (1993) to retrieve molar fraction of the H_2O, CO_2 and CH_4 species. The relative permittivity of non-polar COH species (no permanent dipole moment) is from Harvey and Lemmon (2005), the values of $(\varepsilon_r)_{H_2O}$ are from Sverjensky et al. (2014) and the mixing rule to compute the polarization of the COH fluid is from Harvey and Prausnitz (1987) (*cf.* Appendix A for uncertainties associated to these estimates). Profiles at 0.5, 1, 1.5 and 2.5 GPa are provided in (**c**) showing the non-linear up-T evolution of $(\varepsilon_r)_{mix}$ reflecting increasing dissolution of C. Similar calculation for the simple binary H_2O–CO_2 system (EoS from Holland and Powell, 1991, 1998, 2003) is provided as indication in Supplementary Material, SOM F1. **b**. Contour plot of the pH (pH_w) of pure H_2O (black) at neutrality as defined by $a(H^+) = a(OH^-)$, *i.e.* $pH_w = pK_w/2$. The dissociation constant of water is from Bandura and Lvov (2006). Also shown is the relative change of pH at neutrality in a molecular mixture ($pH_w^{mix} = (pK_w^{mix} - \log(a(H_2O))/2)$ characterized by $a(H_2O) < 1$ and a reduced water dissociation constant K_w^{mix} (see also Section 4.3, Appendix B and Walther, 1992, for details). Thus, a positive value for the difference $pH_w^{mix} - pH_w$ (blue line) indicates that neutrality in the molecular mixture corresponds to higher pH values than pH_w. The dielectric effect on the increase of pK_w^{mix} is largely dominant over the term dependent on $a(H_2O)$.

(model #1), and the carbon concentration in the fluid phase that is required for graphite saturation (model #2) is shown in Fig. 2.

In order to link the phase relations (Fig. 4) to the charge balance and chemistry of the fluid phase, we assume that the non-electrolyte fluid–rock equilibria are independent of the electrolyte chemistry of the fluid (see Section 2.1). This application is essentially designed to isolate and investigate how constituent minerals contribute to and control the composition and speciation of fluids associated with the rock they form. Other factors – *e.g.*, halogen concentration, which may be internally or externally controlled (*e.g.*, Yardley and Graham, 2002) – can be included but are outside the scope of the present work (Galvez et al., in preparation).

3.2. Electrolyte activity ratios

Fig. 5 is contoured with isolines of $\Xi^{Na^+}_{H^+}$ and $\Xi^{K^+}_{H^+}$ in pure H_2O (model #1, Fig. 5a and c) and in graphite-saturated H_2O (model #2, Fig. 5b and d), in equilibrium with the model pelite (similar plots for the ratio $\Xi^{Ca^{2+}}_{Mg^{2+}}$ can be found in SOM Fig. 2a, b). It illustrates the response of the electrolyte activities in the fluid to variations in P, T and mineral assemblages regardless of fluid speciation. Also shown are three P–T paths: path 1, a model path corresponding to the top of a subducting slab (Syracuse et al., 2010); path 2, isobaric heating in the middle crust; path 3, a model exhumation path from high pressure conditions. Fig. 5a shows that the values of $\Xi^{Na^+}_{H^+}$ display limited sensitivity to T; they are within *ca.* 2 log units (3.6–5.3) over the entire P–T interval. These values are similar to previous calculations involving stoichiometric minerals (Bowers et al., 1984) at comparable conditions: Bowers et al. (1984) obtain $\Xi^{Na^+}_{H^+} \sim 4.7$ at albite–sillimanite–quartz equilibrium (600 °C, 0.5 GPa), as compared to ~4.2 here (Fig. 5a), consistent with the reduced activity of the albite end-member in plagioclase in the present calculations. Similarly, the Ξ values are in agreement (within *ca.* 0.1 log unit) with those found by Manning (1998) at the blueschist–eclogite transition, in spite of his different com-

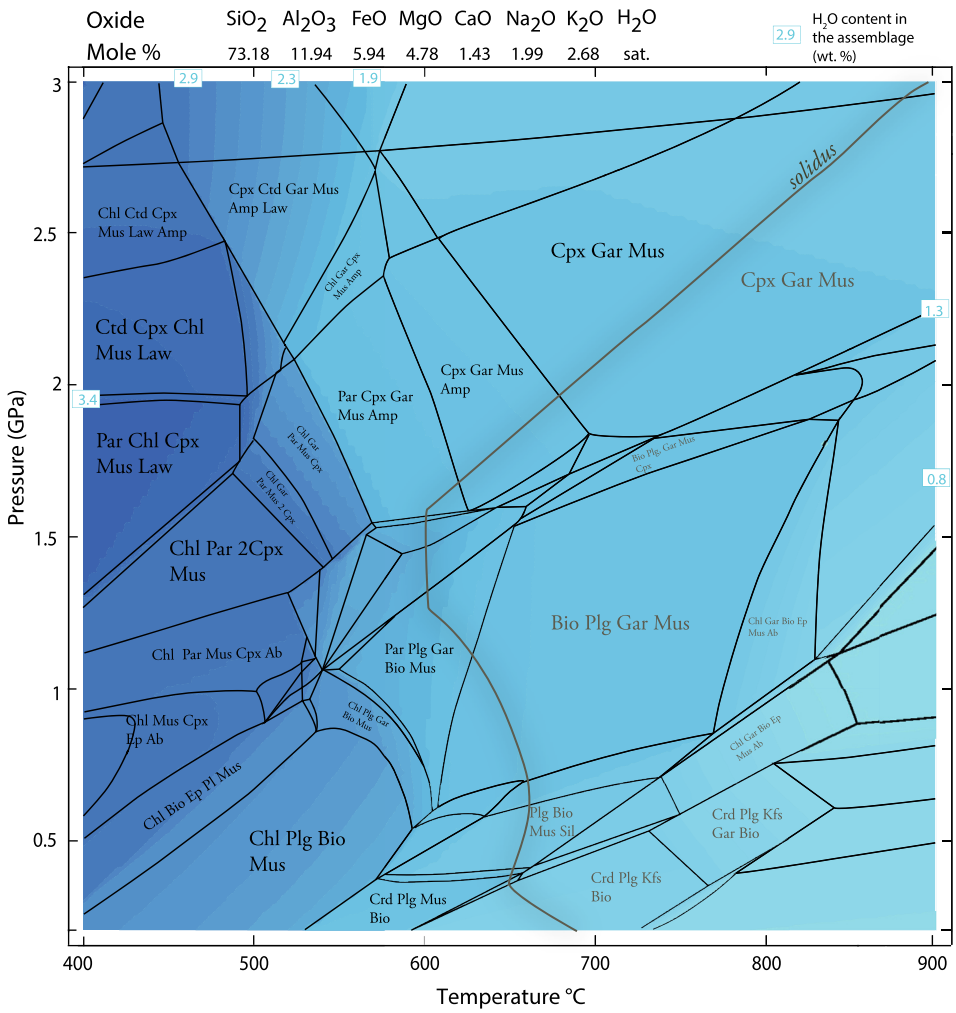

Fig. 4. P–T section in the NCKFMASH system for a model pelite indicating the location of the main mineral assemblages. Blue shading in the background indicates the isopleth of the H_2O content present in the rock at equilibrium (wt%). For example, the 400–600 °C and 1–3 GPa interval correspond to the blueschist–eclogite transition, characterized by significant H_2O loss by the mineral assemblage (>3.4 wt% at blueschist conditions to *ca.* 1.5 wt% H_2O at eclogite conditions) in response to continuous devolatilization of hydrous-phases, *i.e.* lawsonite, chloritoid, chlorite and glaucophane. Black contours delineate distinct mineralogic phase fields and sub-solidus assemblages are indicated in black. Super-solidus assemblages, metastable with respect to a melt phase, are indicated in dark green. The position of the wet-solidus is also indicated. Starting composition is indicated above the figure (adapted from Caddick and Thompson, 2008) and solution models used can be found in Appendix C.

putational approach and restriction to the simple NMASH system (Table 2).

A prominent feature of Fig. 5a, b is the maximum reached by $\Xi_{H^+}^{Na^+}$ along the equilibrium,

$$\underset{\text{(albite in Plg)}}{NaAlSi_3O_8} = \underset{\text{(jadeite in Cpx)}}{NaAlSi_2O_6} + SiO_2 \quad (9)$$

Irrespective of T, an isothermal increase in P leads to an increase of $\Xi_{H^+}^{Na^+}$ to a maximum of ~5.2 in the region of Eq. (9), followed by a decline to values similar to those at low P. This feature and the more subtle variations in $\partial\Xi_{H^+}^{Na^+}/\partial P$ unrelated to Eq. (9) are predominantly controlled by the variation in mode and partial molar volume (v) of Na_2O-bearing phases owing to the relation:

$$\left(\frac{\partial \mu_i}{\partial P}\right)_{T,n_{k\ (k\neq i)}} = \left(\frac{\partial V^{sys}}{\partial n_i}\right)_{P,T,n_{k\ (k\neq i)}} \quad (10)$$

where V^{sys} designates total volume of the fluid–rock system. At $P < 1$ GPa and 500 °C, the main Na_2O bearing phases are plagioclase ($v_{albite} \sim 100$ cm^3/mol at 1 GPa and 500 °C) and white mica ($v_{white\ mica} \sim 139$ cm^3/mol at 0.9 GPa and 500 °C). There is an increase of white mica modal abundance as P rises from 0.2 GPa (22 wt%) to 0.9 GPa (33 wt% white mica), along with a slight increase of Na_2O partitioning in this phase with increasing pressure (from 13.5 to 13.8 wt% Na_2O_{tot}). This feature governs the steady increase in $\Xi_{H^+}^{Na^+}$ over this P–T interval. Conversely, for P greater than ~1 GPa, the lower molar volume of jadeitic clinopyroxene (~60.6 cm^3/mol at 1 GPa and 400 °C) coupled with an up-P increase in its modal abundance leads to the inversion of $\partial\Xi_{H^+}^{Na^+}/\partial P$ to negative values starting at $P \sim 1$ GPa at 400 °C (Eq. (9)) and continuing to higher P (and T) (Figs. 4 and 5). Thus, the $\Xi_{H^+}^{Na^+}$ isolines are chiefly controlled by the isothermal relative evolution of clinopyroxene, plagioclase and white mica solid solution composition.

Values of $\Xi_{H^+}^{K^+}$ (Fig. 5c) display a limited spread (2.6–4.2) over the examined P–T space. Both the variations of this ratio and the isoline slopes show a complex dependence on P, T and phase assemblages. These are tied to white mica and biotite compositions as these are the only major K_2O-bearing phases over most of the P–T range (K-feldspars is only present at $P < 0.7$ GPa and $T > 700$ °C). As with $\Xi_{H^+}^{Na^+}$, values of $\Xi_{H^+}^{K^+}$ show a broad ridge in the vicinity of Eq. (9). At P greater than this equilibrium, isolines generally have positive dP/dT values, reaching *ca.* +10 MPa °C^{-1} in the eclogite facies, and $\Xi_{H^+}^{K^+}$ increases slightly from 3 to 3.8

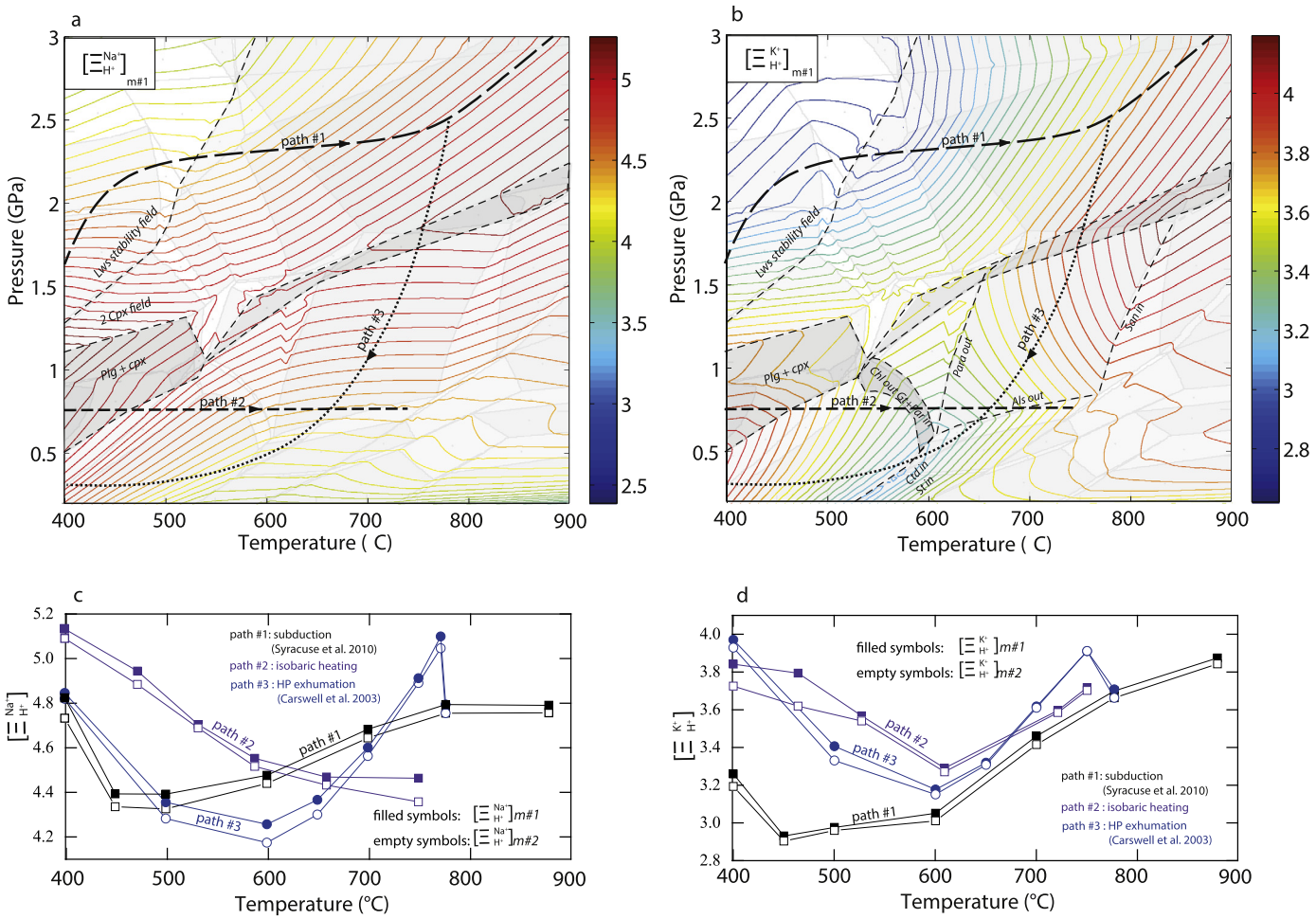

Fig. 5. Contours of activity ratio for selected cations at equilibrium with a devolatilizing metapelite (Fig. 4) for model #1 (pure H_2O) and model #2 (C-saturated COH fluid, $X_O = 1/3$): **a**. $\Xi^{Na^+}_{H^+}$ for model #1. It shows the P dependence of $\Xi^{Na^+}_{H^+}$ ratio, reaching a maximum along equilibrium (11). It also shows the T dependence of $\Xi^{Na^+}_{H^+}$ isolines slopes (see text for details). **b**. $\Xi^{K^+}_{H^+}$ for model #1. The low P domain of biotite–muscovite costability is the prominent feature. In addition, profiles along a subduction (path #1), isobaric heating (path #2), and exhumation (path #3, Carswell et al., 2003) paths for the ratio $\Xi^{Na^+}_{H^+}$ (model #1, filled symbols and model #2, empty symbols) (**c**) and the ratio $\Xi^{K^+}_{H^+}$ (**d**) are indicated. Note that some high-T portions of paths #2 and #3 cross the solidus and would require fluid addition (*ca.* 2 wt%) to maintain equilibrium. This shows the negligible effect of the addition of C on the values and shape of the standard-state variables $\Xi^{Na^+}_{H^+}$ and $\Xi^{K^+}_{H^+}$.

along path 1. At low P, $\Xi^{K^+}_{H^+}$ exhibits a minimum of 3.3 between 500 and 600 °C at $P < 0.5$ GPa in the stability field of Bio + Mus ± Par (Fig. 4).

This valley is characterized by a minimum of the K_2O molar fraction in the muscovite ($X(K_2O^{A\ site}) = K_2O/(K_2O + CaO + Na_2O)^{A\ site}$) of ~0.51 at 590 °C and 0.5 GPa (with 48 wt% of K_2O_{tot} in white mica, 52 wt% of K_2O_{tot} in biotite) compared to ~0.85 at 690 °C (with 22 wt% of K_2O_{tot} in white mica, 78 wt% of K_2O_{tot} in biotite). Simultaneously, biotite abundance in the assemblage increases from ~0.8 wt% at 400 °C and 0.5 GPa, to a maximum of ~29 wt% at 650 °C, and then decreases to ~23 wt% at 690 °C where white mica in the assemblage is replaced by K-feldspar. These variations highlight that entropy changes of assemblages of mineral solid solutions exhibit subtle variations with temperature, leading to isobaric fluctuations of $\partial\Xi^{Na^+}_{H^+}/\partial T$ and $\partial\Xi^{K^+}_{H^+}/\partial T$ owing to:

$$\left(\frac{\partial \mu_i}{\partial T}\right)_{P,n_{k\ (k\neq i)}} = \left(\frac{\partial S^{sys}}{\partial n_i}\right)_{P,T,n_{k\ (k\neq i)}} \tag{11}$$

where S^{sys} designates the total entropy of the fluid–rock system.

In general, the limited spread of values for the two variables $\Xi^{Na^+}_{H^+}$ and $\Xi^{K^+}_{H^+}$ at elevated P and T is remarkable, and suggests that any parameter (*e.g.* pH, see Section 4.3) or process showing strong dependence on $\Xi^{Na^+}_{H^+}$ and/or $\Xi^{K^+}_{H^+}$ may exhibit the same characteristics. However, greater variation in these activity ratios may be expected when additional ligands and controls on fluid composition (*e.g.* presence of chloride) are considered.

The P–T variations in the activity ratios differ only slightly between models #1 and #2. At low P and low T, the values of $\Xi^{K^+}_{H^+}$ and $\Xi^{Na^+}_{H^+}$ obtained with model #2 decrease by only about 5% (Fig. 5c, d) in response to a combination of three factors [Eq. (6)]:

(1) Modifications in the stable phase assemblages. For example, at 450 °C and 0.5 GPa, the modes of biotite and chlorite are respectively 6 and 13.5 wt% in model #1, but 5 and 13.8 wt% in model #2 in response to lowered $a(H_2O)$. In addition, clinopyroxene becomes stable at lower P in model #2.

(2) Change in H_2O chemical potential with added C components.

(3) Modification of the solvent properties of the fluid in the presence of non-polar species.

4. Discussion

4.1. Prediction of solute concentrations

Combining the activity ratios computed above with activity models for solutes and charge balance allows prediction of the

Table 2
Computation results. The ionic strength (I), activity coefficient of monovalent species ($\gamma_{D,1}$), of divalent species ($\gamma_{D,1}$), the pH, the molality of elements and several geochemical indicators (*e.g.* the ratio ([K]+[Na])/[Al]) are provided. These are compared to experimental studies (Wohlers et al., 2011 and Spandler et al., 2007) or modeling work (Manning, 1998).

T (°C)	600			600			600			600			600		
P (GPa)	1.2			2			2.25			2			2.2		
Reference	(a)	this study		(a)	this study		(a)	this study		(b)	this study		(c)	this study	
Chemical system	APQ	APQ		JPQ	JPQ		JPQ	JPQ		NMASH	NCKFMASH		NCKFMASH		
Calculation results			Δ			Δ			Δ						Δ
I		0.06			0.16			0.16			0.17			0.17	
$\gamma_{D,1}$		0.73			0.70			0.71			0.55			0.55	
$\gamma_{D,2}$											0.09			0.09	
pH		6.20			5.75			5.52			5.67			5.50	
Elemental abundance															
log[Na]	−0.67	−1.18	*69*	−0.43	−0.76	*54*	−0.46	−0.77	*51*	−0.40	−0.87		−0.83	−0.87	*8*
log[Al]	−0.81	−1.80	*90*	−0.74	−1.79	*91*	−0.84	−1.87	*91*	−1.80	−1.44		−0.99	−1.54	*72*
log[Si]	−0.02	−0.37	*55*	0.14	−0.22	*57*	0.10	−0.19	*49*	−0.20	−0.22		0.03	−0.19	*41*
log[K]											−1.56		−1.30	−1.65	*56*
log[Ca]											−5.21		−1.43	−4.97	*100*
log[Mg]										−6.00	−5.37		*n.a.*	−5.12	
[Si]/[Al]	6.19	27.19		7.55	37.22		8.83	48.46		39.81	16.75		10.57	22.25	
([K]+[Na])/[Al]	1.39	4.14		2.05	10.77		2.43	12.61		25.12	4.46		1.94	5.50	
[Na]/[Si]	0.22	0.15		0.27	0.29		0.27	0.26		0.63	0.22		0.14	0.21	
[Na]/[K]											4.87		2.95	6.11	
[K]/[Al]											0.76		0.49	0.77	

Notes: The chemical systems are referred to as APG for Albite–Paragonite–Quartz, JPG for Jadeite–Paragonite–Quartz (Wohlers et al., 2011). The values are computed here with bulk composition SiO_2(sat), $Al_2O_3/Na_2O = 1.3$ (molar basis) to produce the Alb–Par–Q or Jd–Par–Q phase assemblages consistent with the experimental system (Wohlers et al., 2011). The Ab → Jd + Q transition is predicted to occur at *ca.* 1.5 GPa at 600 °C. The bulk fluid composition reported by Spandler et al. (2007) has been recalculated, in molal concentration sale, from their Table 5, sample PFI3. The uncertainties on [X] values due to uncertainties in mineral properties is estimated to be *ca.* ±30% of the [Na], [K] and [Al] values, and *ca.* 10% of [Si] values, a conservative estimate. Uncertainties on pH predictions are below 0.1 pH unit (*cf.* Appendix B). The column marked Δ represents the missing quantity of element X, *i.e.* [X], compared to reported experimental values (in %, on a molal basis). The complex $KAlO_{2,aq}$ is included in the calculations leading to the results reported here.
References: (a) Wohlers et al. (2011), (b) Manning (1998), (c) Spandler et al. (2007).

distribution of mass between the rock and the fluid phase implied in each model. We adopt an initial set of ten ionic species (cations Na^+, K^+, Ca^{2+}, Mg^{2+}, $CaOH^+$, $MgOH^+$, H^+ and anions AlO_2^-, OH^-) and seven neutral species ($SiO_{2,aq}$, $Si_2O_{4,aq}$, $NaOH_{aq}$, $NaHSiO_{3,aq}$, $NaAlO_{2,aq}$, KOH_{aq}, $HAlO_{2,aq}$), where $SiO_{2,aq}$ and $Si_2O_{4,aq}$ respectively denote the silica monomer and dimer. Each species is linked to an equation of a form similar to Eq. (6). We assume that silica occurs only as neutral species due to uncertainties in the accuracy of thermochemical data of $HSiO_3^-$ over the P–T range investigated. However, as a check, the calculations were repeated including $HSiO_3^-$, for which data are from Sverjensky et al. (1997). We also neglected the positively charged Al species Al^{3+}, $AlOH^{2+}$, and AlO^+ because trial calculations revealed neutral to alkaline pH values at which these species had relatively low concentrations. Activity coefficients of charged species in the fluid ($\gamma_{D,j}$) were calculated using the Davies equation (Appendix B). Activity coefficients for neutral complexes were assumed equal to 1. The equilibrium constant K_w of the water dissociation (ionization) reaction

$$H_2O = H^+ + OH^- \tag{12}$$

is taken from the most recent estimate proposed by Bandura and Lvov (2006) in model #1. In model #2, it is modified (K_w^{mix}) using our estimates of $(\varepsilon_r)_{mix}$ to account for its deviation from K_w in pure water [*e.g.*, Fig. 3b and Appendix B]. Charge balance provides the last constraint on the system:

$$\sum_j Z_j m_j = 0 \tag{13}$$

where Z_j is the ionic charge. Under these conditions, a system of 12 non-linear equations for model #1, and 17 equations for model #2, can be iteratively solved for H^+ activity, as well as for each electrolyte molalities in the fluid (Appendix B).

The resulting values for the molalities of a range of elements are reported for selected P and T in Table 2. Element abundance are found in the order [Si] > [Na], [Al] ≈ [K] > [Ca] > [Mg], and the ionic strength (I) varies between 10^{-3} (low P) and 1 over most of the P–T space investigated, with a mean *ca.* $I = 0.15$. The steady decrease in [Ca]/[Mg] (and $\Xi_{Mg^{2+}}^{Ca^{2+}}$) with rising T indicates that elevated [Ca] relative to [Mg] may be characteristic of low P–T environments, whereas higher [Mg] relative to [Ca] occurs over a broad range of high metamorphic P and T (SOM Fig. 2). Along with increasing [Si] with rising P–T, our model shows that Si is increasingly partitioned in the dimer with rising T and decreasing P (SOM Fig. 3), and attain equipartition between Si-monomers and Si-dimers at 700 °C and 1 GPa (see also Manning et al., 2010). Thus, the fraction of Si-dimer tracks the decreasing values of $(\varepsilon_r)_{H_2O}$ (Fig. 1), and our results are in qualitative conformity with the numerous field evidence for preferential mobility of Si, alkali (Na, K) or Al in crustal or slab fluids (*e.g.*, Bebout and Barton, 1993; Penniston-Dorland and Ferry, 2008; Bucholz and Ague, 2010; Galvez et al., 2013b), sometimes precipitated in kyanite + quartz (±omphacite) (*e.g.* Widmer and Thompson, 2001; Bucholz and Ague, 2010) or albite + quartz veins (*e.g.*, Bucholz and Ague, 2010).

4.2. Comparison between predicted and experimental determinations of fluid composition

The comparison of our predictions with experimental studies can provide valuable information about solute associations not yet considered in current thermochemical modeling of fluid speciation. The thermochemical data for aqueous silica (Sverjensky et al., 2014) accurately reproduce quartz solubility and silica speciation at elevated P and T (Manning, 1994; Zotov and Keppler, 2000; Mysen, 2010). However, uncertainties in the data for $HSiO_3^-$ prevent rigorous assessment of the contribution of dissolved silica to

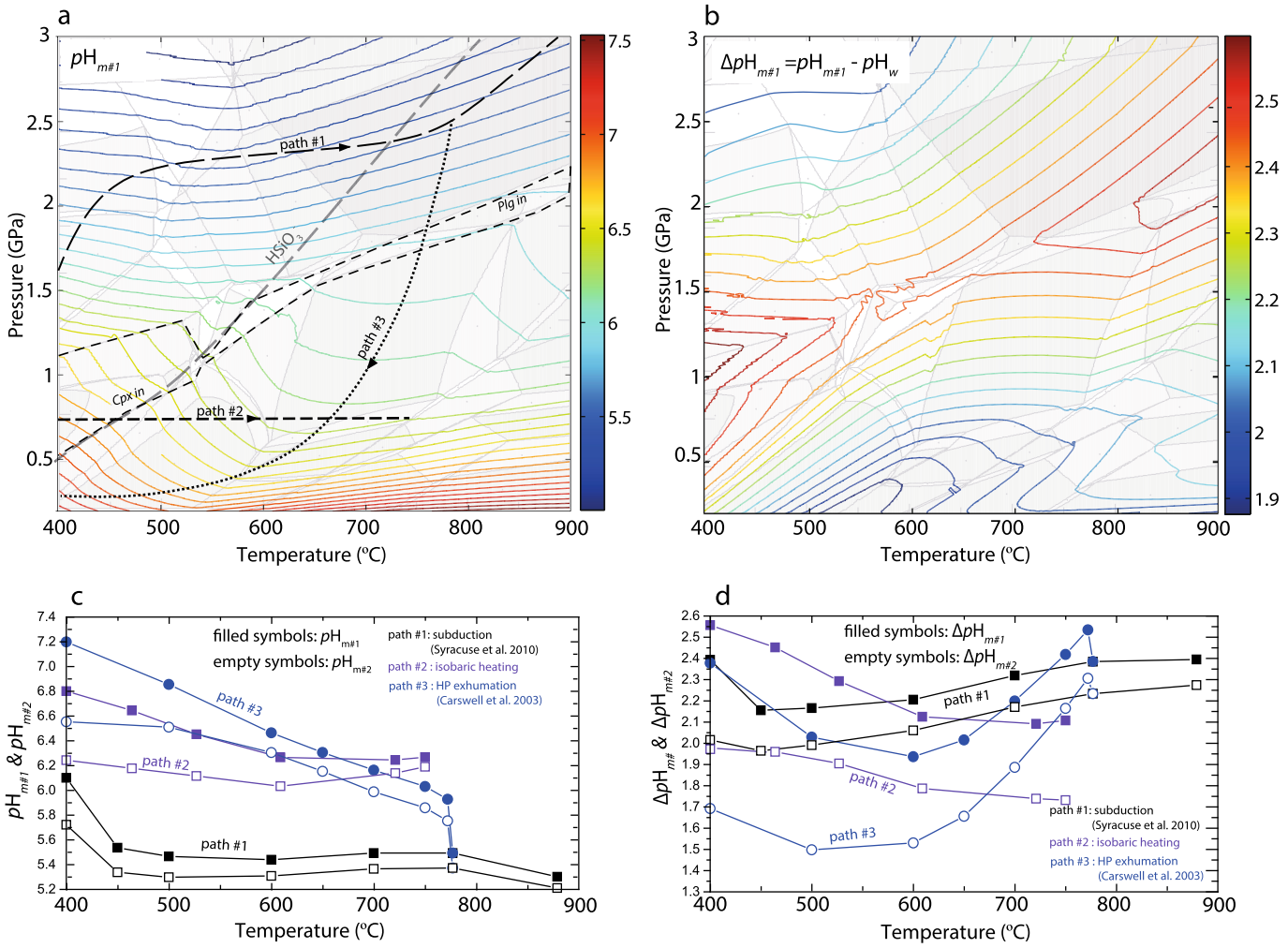

Fig. 6. a. Equilibrium pH computed by solving Eqs. (6), (12), (13) for the modeled metapelite in model #1 (filled symbols). **b**. This panel shows the pH difference $\Delta p\mathrm{H}_{m\#1} = p\mathrm{H}_{m\#1} - p\mathrm{H}_w$. It is a measure of the *alkalinity* (or acidity) of the equilibrium fluid relative to neutrality $p\mathrm{H}_w$ (Fig. 3). The values show a broad maximum at the location of Eq. (9), and decrease at P–T conditions further away from this equilibrium. The difference $\Delta p\mathrm{H}_{m\#2} = p\mathrm{H}_{m\#2} - p\mathrm{H}_w^{mix}$ is the *alkalinity* of the equilibrium fluid (model #2), computed relative to acid–base neutrality in the mixture $p\mathrm{H}_w^{mix}$ (*cf.* Fig. 3, text and Appendix B for details). The profile of $p\mathrm{H}_{m\#1}$ (filled symbols) and $p\mathrm{H}_{m\#2}$ (empty symbols) and $\Delta p\mathrm{H}_{m\#1}$ and $\Delta p\mathrm{H}_{m\#2}$ are reproduced along three P–T paths in **c** and **d** respectively. The trends show that addition of C affects the pH in a complex fashion.

the overall charge balance of the fluid and introduce some uncertainties on the total Si solubility at these alkaline conditions. At low T and elevated P, neutral silica monomers and polymers are most probably metastable, to a certain extent, with respect to $HSiO_3^-$, as revealed by repeating the calculations using the available thermochemical data for this anion. Similarly, the data for $HAlO_{2,aq}$ and AlO_2^- are from Sverjensky et al. (2014), and those of $KAlO_{2,aq}$ from Pokrovskii and Helgeson (1997). Using these species, Sverjensky et al. (2014) report good reproducibility of corundum solubility in a wide range of P–T conditions, at both neutral (*e.g.*, Tropper and Manning, 2007), and alkaline conditions (*i.e.* Wohlers and Manning, 2009). Regardless, our prediction for the fluid peralkalinity at 600 °C and 2.2 GPa, *ca.* $([Na]+[K])/[Al] \sim 12$, or for the [Si]/[Al] ratio, *ca.* 50, remain relatively remote from experimental measurements at similar conditions, *e.g.* $([Na]+[K])/[Al] \sim 2$, and $[Si]/[Al] \sim 10$, by Spandler et al. (2007). Including a K–Al complex $KAlO_{2,aq}$ to model #1 somewhat reduces the difference between our predictions, *e.g.* $([Na]+[K])/[Al] \sim 6$, $[Si]/[Al] \sim 20$, and the experimental values, but a substantial discrepancy that exceeds uncertainties due to mineral or solute thermochemical properties persists, pointing to the existence of metal-complexes and/or alkali-aluminosilicate polymers not accounted for in the present speciation. These additional K–Al, K–Si and K–Al–Si species represent an important fraction of [Al] and [K], *i.e.* 60 to 85% of their total solubility, at 600 °C and 2.2 GPa (Table 2). Similarly, solutes are needed to explain the discrepancies observed for [Ca] and [Mg]. Notably, this appears to be a feature characteristic of high P fluids. For example, Pak et al. (2003) determined the solubility of the pelitic assemblage albite + K feldspar + andalusite + quartz in aqueous chloride solutions at 600 and 650 °C, 0.2 GPa, and found it unnecessary to invoke additional species to K–Al and K–Si complexes to explain their results.

Wohlers et al. (2011) investigated the solubility of albite/jadeite–paragonite–quartz in H_2O at 500 and 600 °C and a range of P. Applying our method to this simplified system returns values for both [Na] and [Al] that are underestimated (model #1) by 0.17 ± 0.02 molal, and [Si] by 0.55 ± 0.05 molal at all conditions (this deficit represents *ca.* 50% of [Na], [Si] and 90% of [Al], Table 2).

4.3. Rock control on pH variations

The pH in model #1 is alkaline over the investigated P–T range (Fig. 6a), with values up to *ca.* 2.6 log units over neutral pH in the vicinity of equilibrium (9) (Fig. 6b). The *alkalinity* ($\Delta p\mathrm{H}_{m\#1}$) of the fluid is the difference between buffered pH ($p\mathrm{H}_{m\#1}$) and acid–base neutrality [*i.e.* $p\mathrm{H}_w$ corresponding to the condition $a(H^+) = a(OH^-)$, Eq. (12), and Fig. 3b], thus $\Delta p\mathrm{H}_{m\#1} = p\mathrm{H}_{m\#1} - p\mathrm{H}_w$. As predicted based on alkali activity ratios (Fig. 5), pH is relatively

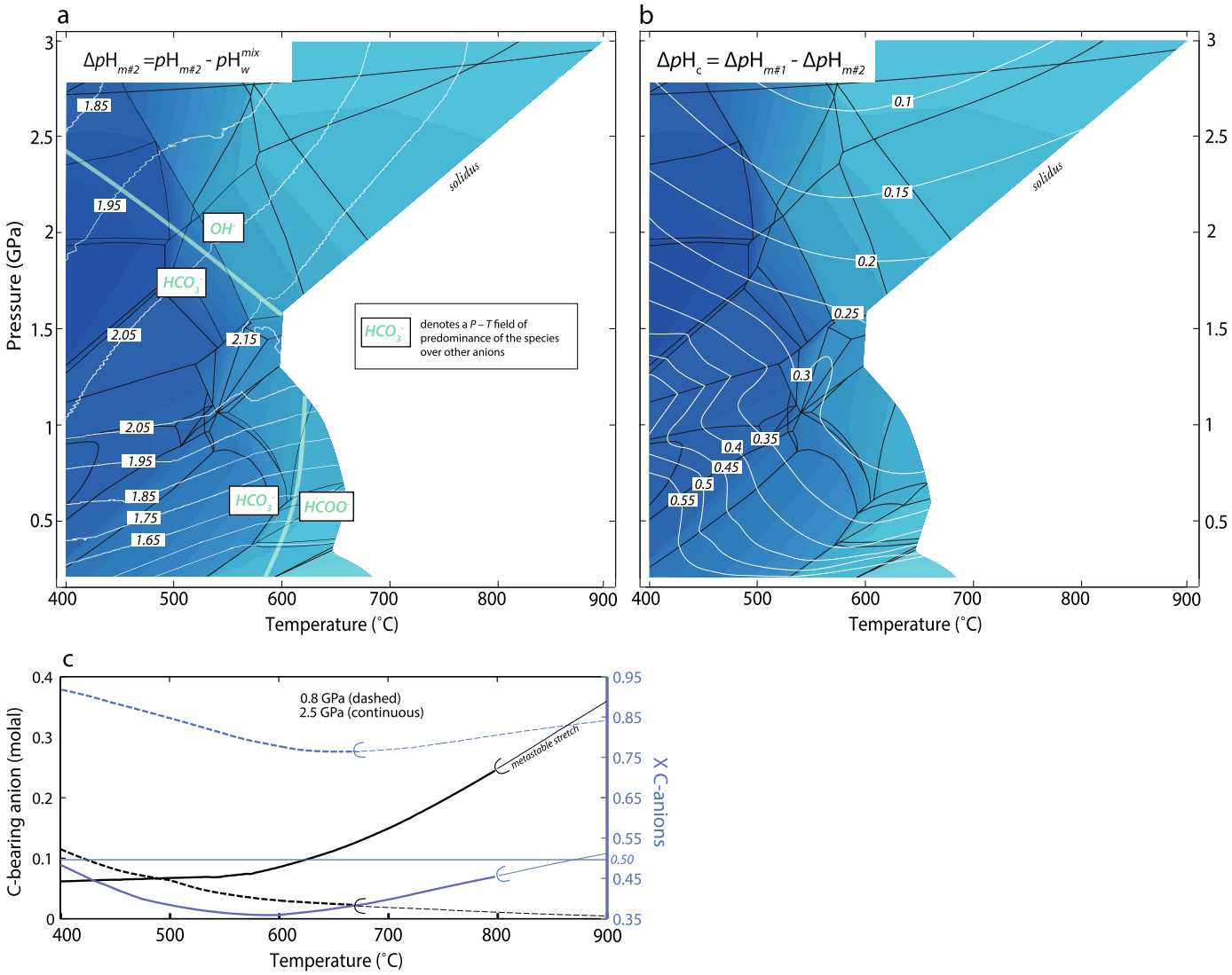

Fig. 7. a. Contours of $\Delta pH_{m\#2}$. The predominant ligands are indicated along with their P–T field of predominance (thick pale-green line). The water content of the rock (blue shading) and the main mineral stability fields (black lines) are also indicated. Details can be found in Fig. 4. **b**. Contours of $\Delta pH_c = \Delta pH_{m\#1} - \Delta pH_{m\#2}$, a measure for the *relative alkalinity* of the fluid between model #1 (pure H_2O) and model #2 (COH fluid at $X_O = 1/3$) compared to neutrality, independently defined in both cases (Fig. 6). Only the sub-solidus field is represented in (a) and (b). **c**. Concentration of C-bearing anions in the fluid (black lines, including CO_3^{2-}, HCO_3^-, $NaCO_3^-$ and $HCOO^-$) at 0.8 GPa (dashed), and 2.5 GPa (continuous), and corresponding fraction of C-bearing anions (in % of total anions, blue lines). It shows a disconnect between the total C content (Fig. 2), abundance and molar fraction of C-bearing anion in a COH fluid at equilibrium with a metapelite. It should be noted that in the presence of carbonates, or of conditions more oxidizing than those prevailing at $X_O = 1/3$, the molar fraction carbon and oxygen [$Y_C = n_C/(n_C + n_O + n_H)$ and $Y_O = n_O/(n_C + n_O + n_H)$] increase in the fluid (*e.g.*, Connolly and Cesare, 1993). This should result in the increase of the abundance of C-bearing anions in the fluid and to larger ΔpH_c values.

uniform along P–T paths 1 and 2. By contrast, pH fluctuations span *ca*. 2 log units along typical high P exhumation paths. Na^+ and OH^- are the predominant charge balancing species in model #1 (Fig. 6). The anionic species $HSiO_3^-$ also contributes at elevated P and low T (upper-left quadrant in Figs. 4–7). This is supported by the observation that the couple Na^+–$HSiO_3^-$ predominates at blueschist–eclogite facies conditions (Fig. 6a) when $HSiO_3^-$ is added to the calculation. The increased abundance of OH^- at elevated P–T conditions (Fig. 3b) may favor the formation of hydroxo-metal complexes of economic interest, supporting a mechanism previously hypothesized by Hack and Mavrogenes (2006) (*cf.* Seward et al., 2014). A possible role for silica in trace element complexing via formation of $[M^{n+}HSiO_3^-]^{(n-1)+}$ complex at elevated P, *i.e.* blueschist to eclogite facies, may also be proposed, and future experimental works are needed to validate this hypothesis. The effect of isothermal P increase or decrease from the position of Eq. (9) is to bring the fluid closer to neutrality. The temperature dependence of $\Delta pH_{m\#1}$ increases as geothermal gradients become steeper. Thus, moderate variations $\Delta pH_{m\#1}$ are predicted along the isobaric heating (path #2, Fig. 6d) and the prograde subduction paths. Larger variations are predicted by burial along high P exhumation. These display a U shape pattern inherited from the patterns of $\Xi^{Na^+}_{H^+}$ and $\Xi^{K^+}_{H^+}$ (Fig. 5a, b).

The addition of C (model #2) induces important pH differences in the fluid relative to those found in model #1 at the same conditions. Values of pH are lower (Fig. 6a) and systematically closer to neutrality (*i.e.* Fig. 3b) in model #2 than in model #1 at all P and T conditions (Figs. 6d and 7a, b). That is, the *relative alkalinity*, defined here as $\Delta pH_c = \Delta pH_{m\#1} - \Delta pH_{m\#2}$ with $\Delta pH_{m\#2} = pH_{m\#2} - pH^{mix}_w$ (Figs. 3b, 7a), is everywhere positive and span the range 0.1 to 0.6 (Fig. 7b). Yet, we observe that this effect becomes less pronounced (ΔpH_c diminishes) as P and T rise along isolines of C molalities (Fig. 2). These changes can be ascribed to (1) modifications induced to mineral compositions by virtue of Eq. (6), (2) modification of the fluid speciation by the presence of additional C-bearing ions, *e.g.*, HCO_3^-, $HCOO^-$, $NaCO_3^-$,

$CaHCO_3^+$ and CO_3^{2-}, (3) modification of the solvent properties. The first (mineralogic) and second (speciation) factors are dominant at $T < 600\,^{\circ}C$ where the ΔpH_c isolines are tied to the main phase boundaries. However, both effects on the decrease of the fluid alkalinity at low T are dampened, until *ca.* 600 °C, by the progressive decrease of $(\varepsilon_r)_{mix}$ (Fig. 3a), and its effect on the decrease of CO_2 ionization (*e.g.*, Wen and Olesik, 2000). This is reflected in the drop of the molar fraction of C-bearing anions in the fluid (Fig. 7c) to *ca.* 600 °C. With further heating ($T > 600\,^{\circ}C$), the isobaric increase of ΔpH_c parallels the increasing fraction of C-bearing anions of intermediate C valence state (predominantly $HCOO^-$ at $T > 600\,^{\circ}C$ and $P < 2$ GPa) in the total anion budget of the fluid (Fig. 7c), simultaneously to the decrease of their concentration and of the ionic strength, and despite the dramatic increase of C solubility (Figs. 1–3). The ionic strength is similar within uncertainty between model #1 and #2 at $P > 1.5$ GPa. However, model #2 returns an ionic strength ca. 4 times higher at low T and low P, and lower by 1–2 orders of magnitude at elevated T and low P than that of model #1. The formation of $HCOO^-$ is favored by the up-T isobaric increase of $f(H_2)$ at constant X_O, a redox-dependent mechanism that would require experimental validation. We also find that the bicarbonate ion predominates over other anions in this model at low T and up to *ca.* 2 GPa, a domain where C molality (*ca.* 0.02 to 2 molal) and $(\varepsilon_r)_{mix}$ (*ca.* 15 to 40) are both high enough to favor the presence of ionic C-bearing ligands. Conversely, at $P = 2.5$ GPa and low T, the amount of C bearing anions in the fluid is similar to that at 0.8 GPa (Fig. 7c), increases towards elevated T conditions, but is never predominant in the anionic budget of the fluid. Owing to alkaline pH, the existence of this ionic C pool increases [C] by a factor 2 to 10 ([C] ~0.1 molal) at 2–3 GPa and 400–500 °C (SOM Fig. 4) compared to estimates from a purely molecular model (Connolly and Cesare, 1993, *cf.* Fig. 2 and SOM Fig. 4).

5. Conclusion

[1] This work presents a new route to retrieve information on aqueous speciation by bridging conventional chemical petrology with mixed-solvent solution chemistry. It is applicable to a range of rock-dominated high-pressure conditions, including subduction zones. The comparison of predictions from such a model with independent experimental data offers a unique window into elusive processes of ionic association at elevated P and T. Enhancing the accuracy of such predictions requires continued improvement of the consistency between mineral and solute thermochemical data sets (*cf.* Sverjensky et al., 1991; Holland and Powell, 1998, p. 314; and Appendix B).

[2] Na-bearing mineral solid-solutions exert the main petrologic control on the acid–base budget of fluids in the models investigated. Thus, our results highlight a decoupling between the abundance of major/minor element in rocks (Na_2O *ca.* 2 wt% here), and their role on fluid speciation and properties. Predicted pH for both models is alkaline at low P but is closer to neutrality as P increases above the albite–jadeite–quartz transition. It shows little variation along subduction or isobaric heating P–T paths, and large fluctuations of up to 2 log units along model retrograde paths.

[3] The decrease of $(\varepsilon_r)_{mix}$ in COH fluids dampens H_2O and CO_2 ionization. Combined with the presence of additional C bearing ligands, the overall effect of C is to bring the pH of the system closer to neutrality by up to *ca.* 0.6 pH at low T and P. C-bearing anions, *i.e.* HCO_3^- (and $HCOO^-$), are the dominant ligands at low P despite their limited amount in the fluid. These also represent a non-negligible fraction (up to *ca.* 50%) of the total anion budget at elevated P and T. Although few studies have experimentally determined the role of aqueous C on major and trace elements complexation at elevated P and T conditions relevant for subduction zones (Tsay et al., 2014), our work highlights that C-bearing ligands may be available for this purpose. Understanding the full implications of these redox–electrostatic processes on the behavior, budget and recyling of C–N–S volatiles and their isotopes (*e.g.*, Hayes and Waldbauer, 2006), and on ore-metal complexation, transport and deposition (*e.g.* Phillips and Evans, 2004) to upper mantle P and T is of fundamental importance.

[4] The existence of Al–Si and alkali–Al–Si polymer has long been inferred in simple mineral–fluid systems (*e.g.*, Manning et al., 2010). By comparing our results to experimental solubility data, we extend this conclusion to more complex compositional systems, and suggest that metal complex and polymerized species may be more numerous than has previously been appreciated. We show that Ca, Mg, K–Si and K–Al–Si species are required. The extent of these discrepancies, in particular for Ca and Mg, calls for dedicated experimental characterization and/or first-principles MD simulation of the stoichiometric, charge and thermochemical properties of these species. This would be a decisive step toward the accurate quantification of the interactions between compositionally variable lithologies (*e.g.*, Konrad-Schmolke et al., 2011; Galvez et al., 2013b; Marchesi et al., 2013; Angiboust et al., 2014) and complex aqueous solutions associated to deep Earth metasomatism, while preserving a physically realistic model of fluid speciation.

[5] Future applications of our method to natural systems will require additional considerations: carbonate, sulfate, sulfides, phosphates, borate, multicomponent polymeric anions, and halogen (*e.g.*, Newton and Manning, 2010) can all exert important roles as charge-balancing anions and as ligands. The present study lays the foundation for future works investigating the consequence of these additional sources of complexity on the composition and speciation of metamorphic fluids.

Acknowledgements

We are indebted to Deborah Smith, Allan Harvey, Mark Caddick, Paul Asimow and Dimitri Sverjensky for providing valuable insights on various computational or theoretical aspects of this work at an early stage of the project. We thank Lucie Tajcmanova, Chris Glein, Xin Zhong, David Dolejs, Nikolai Akinfiev, George Cody, Peter Ulmer, Jay Ague, Dan Miron and Shuhei Ohara for helpful discussions. The authors wish to acknowledge thorough reviews by John Walther and Bruce Yardley that substantially improved this manuscript, as well as helpful reviews by Simone Tumiati and Isabelle Daniel. We thank B. Marty for editorial guidance and handling. This project was conceived and conducted at the Geophysical Laboratory (CIW) where the first author benefited from a Carnegie Fellowship. A NASA early career collaboration award and an ETH fellowship ETH/CoFUND Fel-06 13-2 (M.E.G.), the US National Science Foundation grant EAR 1347987 (C.E.M.), and support from Deep Carbon Observatory are gratefully acknowledged.

Appendix. Supplementary material

Supplementary material related to this article can be found online at http://dx.doi.org/10.1016/j.epsl.2015.06.019.

References

Ague, J.J., 1994. Mass transfer during Barrovian metamorphism of pelites, south-central Connecticut; I, Evidence for changes in composition and volume. Am. J. Sci. 294 (8), 989–1057.

Ague, J.J., Nicolescu, S., 2014. Carbon dioxide released from subduction zones by fluid-mediated reactions. Nat. Geosci. 7 (5), 355–360.

Andersen, T., Burke, E.A.J., Austrheim, H., 1989. Nitrogen-bearing, aqueous fluid inclusions in some eclogites from the Western Gneiss Region of the Norwegian Caledonides. Contrib. Mineral. Petrol. 103 (2), 153–165.

Angiboust, S., Pettke, T., De Hoog, J.C., Caron, B., Oncken, O., 2014. Channelized fluid flow and eclogite-facies metasomatism along the subduction shear zone. J. Petrol. 55 (5), 883–916.

Aranovich, L.Y., Newton, R.C., 1999. Experimental determination of CO_2–H_2O activity–composition relations at 600–1000 °C and 6–14 kbar by reversed decarbonation and dehydration reactions. Am. Mineral. 84, 1319–1332.

Archer, D.G., Wang, P., 1990. The dielectric constant of water and Debye–Hückel limiting law slopes. J. Phys. Chem. Ref. Data 19, 371–411.

Bandura, A.V., Lvov, S.N., 2006. The ionization constant of water over wide ranges of temperature and density. J. Phys. Chem. Ref. Data 35, 15–30.

Bebout, G.E., Barton, M.D., 1993. Metasomatism during subduction: products and possible paths in the Catalina Schist, California. Chem. Geol. 108 (1), 61–92.

Botti, A., Bruni, F., Mancinelli, R., Ricci, M.A., Lo Celso, F., Triolo, R., Ferrante, F., Soper, A.K., 2008. Study of percolation and clustering in supercritical water–CO_2 mixtures. J. Chem. Phys. 128 (16), 164504.

Bowers, T.S., Jackson, K.J., Helgeson, H.C., 1984. Equilibrium Activity Diagrams: For Coexisting Minerals and Aqueous Solutions at Pressures and Temperatures to 5 kb and 600 °C. Springer, Berlin.

Bucholz, C.E., Ague, J.J., 2010. Fluid flow and Al transport during quartz-kyanite vein formation, Unst, Shetland Islands, Scotland. J. Metamorph. Geol. 28, 19–39.

Caciagli, N.C., Manning, C.E., 2003. The solubility of calcite in water at 6–16 kbar and 500–800 °C. Contrib. Mineral. Petrol. 146, 275–285.

Caddick, M.J., Thompson, A.B., 2008. Quantifying the tectono-metamorphic evolution of pelitic rocks from a wide range of tectonic settings: mineral compositions in equilibrium. Contrib. Mineral. Petrol. 156, 177–195.

Carswell, D.A., Brueckner, H.K., Cuthbert, S.J., Mehta, K., O'Brien, P.J., 2003. The timing of stabilisation and the exhumation rate for ultra-high pressure rocks in the Western Gneiss Region of Norway. J. Metamorph. Geol. 21 (6), 601–612.

Connolly, J.A.D., Cesare, B., 1993. C–O–H–S fluid composition and oxygen fugacity in graphitic metapelites. J. Metamorph. Geol. 11, 379–388.

Dandurand, J.L., Schott, J., 1992. Prediction of ion association in mixed-crustal fluids. J. Phys. Chem. 96, 7770–7777.

Deul, R., Franck, E., 1991. The static dielectric constant of the water–benzene mixture system to 400 °C and 2800 bar. Ber. Bunsenges. Phys. Chem. 95, 847–853.

Dolejš, D., 2013. Thermodynamics of aqueous species at high temperatures and pressures: equations of state and transport theory. Rev. Mineral. Geochem. 76 (1), 35–79.

Dolejš, D., Manning, C.E., 2010. Thermodynamic model for mineral solubility in aqueous fluids: theory, calibration and application to model fluid–flow systems. Geofluids 10 (1–2), 20–40.

Dubessy, J., Moissette, A., Bakker, R.J., Frantz, J.D., Zhang, Y.G., 1999. High-temperature Raman spectroscopic study of H_2O–CO_2–CH_4 mixtures in synthetic fluid inclusions; first insights on molecular interactions and analytical implications. Eur. J. Mineral. 11, 23–32.

Evans, K.A., Gordon, R.A., Mavrogenes, J.A., Tailby, N., 2009. The effect of CO_2 on the speciation of RbBr in solution at temperatures to 579 °C and pressures to 0.26 GPa. Geochim. Cosmochim. Acta 73 (9), 2631–2644.

Evans, K.A., Phillips, G.N., Powell, R., 2006. Rock-buffering of auriferous fluids in altered rocks associated with the golden mile-style mineralization, Kalgoorlie Gold Field, Western Australia. Econ. Geol. 101, 805–817.

Fernandez, D.P., Goodwin, A.R.H., Lemmon, E.W., Sengers, J.L., Williams, R.C., 1997. A formulation for the static permittivity of water and steam at temperatures from 238 K to 873 K at pressures up to 1200 MPa, including derivatives and Debye–Hückel coefficients. J. Phys. Chem. Ref. Data 26 (4), 1125–1166.

Frezzotti, M.L., Selverstone, J., Sharp, Z.D., Compagnoni, R., 2011. Carbonate dissolution during subduction revealed by diamond-bearing rocks from the Alps. Nat. Geosci. 4 (10), 703–706.

Fyfe, W.S., Price, N.J., Thompson, A.B., 1978. Fluids in the Earth's Crust. Elsevier, Amsterdam.

Galvez, M.E., Beyssac, O., Martinez, I., Benzerara, K., Chaduteau, C., Malvoisin, B., Malavieille, J., 2013a. Graphite formation by carbonate reduction during subduction. Nat. Geosci. 6, 473–477.

Galvez, M.E., Martinez, I., Beyssac, O., Benzerara, K., Agrinier, P., Assayag, N., 2013b. Metasomatism and graphite formation at a lithological interface in Malaspina (Alpine Corsica, France). Contrib. Mineral. Petrol. 166, 1687–1708.

Hack, A.C., Mavrogenes, J.A., 2006. A synthetic fluid inclusion study of copper solubility in hydrothermal brines from 525 to 725 °C and 0.3 to 1.7 GPa. Geochim. Cosmochim. Acta 70, 3970–3985.

Harvey, A.H., Lemmon, E.W., 2005. Method for estimating the dielectric constant of natural gas mixtures. Int. J. Thermophys. 26, 31–46.

Harvey, A.H., Prausnitz, J.M., 1987. Dielectric constants of fluid mixtures over a wide range of temperature and density. J. Solution Chem. 16, 857–869.

Hayes, J.M., Waldbauer, J.R., 2006. The carbon cycle and associated redox processes through time. Philos. Trans. R. Soc. B, Biol. Sci. 361 (1470), 931–950.

Helgeson, H.C., 1968. Evaluation of irreversible reactions in geochemical processes involving minerals and aqueous solutions – I. Thermodynamic relations. Geochim. Cosmochim. Acta 32, 853–877.

Helgeson, H.C., Kirkham, D.H., 1976. Theoretical prediction of the thermodynamic properties of aqueous electrolytes at high pressures and temperatures. III. Equation of state for aqueous species at infinite dilution. Am. J. Sci. 276, 97–240.

Helgeson, H.C., Kirkham, D.H., Flowers, G.C., 1981. Theoretical prediction of the thermodynamic behavior of aqueous electrolytes by high pressures and temperatures. IV. Calculation of activity coefficients, osmotic coefficients, and apparent molal and standard and relative partial molal properties to 600 °C and 5 kb. Am. J. Sci. 281, 1249–1516.

Holland, T., Powell, R., 1991. A Compensated-Redlich–Kwong (CORK) equation for volumes and fugacities of CO_2 and H_2O in the range 1 bar to 50 kbar and 100–1600 °C. Contrib. Mineral. Petrol. 109, 265–273.

Holland, T., Powell, R., 2003. Activity-composition relations for phases in petrological calculations: an asymmetric multicomponent formulation. Contrib. Mineral. Petrol. 145, 492–501.

Holland, T.J.B., Powell, R., 1998. An internally consistent thermodynamic data set for phases of petrological interest. J. Metamorph. Geol. 16, 309–343.

Kirkwood, J.G., 1939. The dielectric polarization of polar liquids. J. Chem. Phys. 7, 911–919.

Konrad-Schmolke, M., Zack, T., O'Brien, P.J., Barth, M., 2011. Fluid migration above a subducted slab—Thermodynamic and trace element modelling of fluid–rock interaction in partially overprinted eclogite-facies rocks (Sesia Zone, Western Alps). Earth Planet. Sci. Lett. 311 (3), 287–298.

Landau, L.D., Lifshitz, M., 1960. Electrodynamics of Continuous Media. Pergamon Press, Oxford.

Looyenga, H., 1965. Dielectric constants of heterogeneous mixtures. Physica 31, 401–406.

Malvoisin, B., Chopin, C., Brunet, F., Galvez, M.E., 2012. Low-temperature wollastonite formed by carbonate reduction: a marker of serpentinite redox conditions. J. Petrol. 53 (1), 159–176.

Manning, C.E., 1994. The solubility of quartz in H_2O in the lower crust and upper mantle. Geochim. Cosmochim. Acta 58, 4831–4839.

Manning, C.E., 1998. Fluid composition at the blueschist–eclogite transition in the model system Na_2O–MgO–Al_2O_3–SiO_2–H_2O–HCl. Schweiz. Mineral. Petrogr. Mitt. 78, 225–242.

Manning, C.E., Antignano, A., Lin, H.A., 2010. Premelting polymerization of crustal and mantle fluids, as indicated by the solubility of albite + paragonite + quartz in H_2O at 1 GPa and 350–620 °C. Earth Planet. Sci. Lett. 292, 325–336.

Marchesi, C., Garrido, C.J., Padrón-Navarta, J.A., Sánchez-Vizcaíno, V.L., Gómez-Pugnaire, M.T., 2013. Element mobility from seafloor serpentinization to high-pressure dehydration of antigorite in subducted serpentinite: insights from the Cerro del Almirez ultramafic massif (southern Spain). Lithos 178, 128–142.

Marshall, W.L., Franck, E.U., 1981. Ion product of water substance, 0–1000 °C, 1–10,000 bars new international formulation and its background. J. Phys. Chem. Ref. Data 10, 295–304.

Mottl, M.J., Wheat, C.G., Fryer, P., Gharib, J., Martin, J.B., 2004. Chemistry of springs across the Mariana forearc shows progressive devolatilization of the subducting plate. Geochim. Cosmochim. Acta 68 (23), 4915–4933.

Mysen, B.O., 2010. Speciation and mixing behavior of silica-saturated aqueous fluid at high temperature and pressure. Am. Mineral. 95, 1807–1816.

Newton, R.C., Manning, C.E., 2010. Role of saline fluids in deep-crustal and upper-mantle metasomatism: insights from experimental studies. Geofluids 10, 58–72.

Pak, T.M., Hauzenberger, C.A., Baumgartner, L.P., 2003. Solubility of the assemblage albite + K-feldspar + andalusite + quartz in supercritical aqueous chloride solutions at 650 °C and 2 kbar. Chem. Geol. 200, 377–393.

Pan, D., Spanu, L., Harrison, B., Sverjensky, D.A., Galli, G., 2013. Dielectric properties of water under extreme conditions and transport of carbonates in the deep Earth. Proc. Natl. Acad. Sci. USA 110, 6646–6650.

Penniston-Dorland, S.C., Ferry, J.M., 2008. Element mobility and scale of mass transport in the formation of quartz veins during regional metamorphism of the Waits River Formation, east-central Vermont. Am. Mineral. 93 (1), 7–21.

Philippot, P., Selverstone, J., 1991. Trace-element-rich brines in eclogitic veins: implications for fluid composition and transport during subduction. Contrib. Mineral. Petrol. 106 (4), 417–430.

Phillips, G.N., Evans, K.A., 2004. Role of CO_2 in the formation of gold deposits. Nature 429 (6994), 860–863.

Pokrovskii, V.A., Helgeson, H.C., 1997. Thermodynamic properties of aqueous species and the solubilities of minerals at high pressures and temperatures: the system Al_2O_3—H_2O—KOH. Chem. Geol. 137, 221–242.

Schmidt, C., 2014. Raman spectroscopic determination of carbon speciation and quartz solubility in H_2O + Na_2CO_3 and H_2O + $NaHCO_3$ fluids to 600 °C and 1.53 GPa. Geochim. Cosmochim. Acta 145, 281–296.

Seward, T.M., Williams-Jones, A.E., Migdisov, A.A., 2014. The chemistry of metal transport and deposition by ore forming hydrothermal fluids. In: Treatise on Geochemistry, vol. 13, 2nd edition. Elsevier, Amsterdam, pp. 29–57.

Shock, E.L., Oelkers, E.H., Johnson, J.W., Sverjensky, D.A., Helgeson, H.C., 1992. Calculation of the thermodynamic properties of aqueous species at high pressures and temperatures. Effective electrostatic radii, dissociation constants and standard partial molal properties to 1000 °C and 5 kbar. J. Chem. Soc., Faraday Trans. 88, 803–826.

Spandler, C., Mavrogenes, J., Hermann, J., 2007. Experimental constraints on element mobility from subducted sediments using high-P synthetic fluid/melt inclusions. Chem. Geol. 239, 228–249.

Sverjensky, D.A., Harrison, B., Azzolini, D., 2014. Water in the deep Earth: the dielectric constant and the solubilities of quartz and corundum to 60 kb and 1200 °C. Geochim. Cosmochim. Acta 129, 125–145.

Sverjensky, D.A., Hemley, J., d'Angelo, W., 1991. Thermodynamic assessment of hydrothermal alkali feldspar-mica-aluminosilicate equilibria. Geochim. Cosmochim. Acta 55, 989–1004.

Sverjensky, D.A., Shock, E.L., Helgeson, H.C., 1997. Prediction of the thermodynamic properties of aqueous metal complexes to 1000 °C and 5 kb. Geochim. Cosmochim. Acta 61, 1359–1412.

Syracuse, E.M., van Keken, P.E., Abers, G.A., 2010. The global range of subduction zone thermal models. Phys. Earth Planet. Inter. 183, 73–90.

Tanger, J.C., Helgeson, H.C., 1988. Calculation of the thermodynamic and transport properties of aqueous species at high pressures and temperatures; revised equations of state for the standard partial molal properties of ions and electrolytes. Am. J. Sci., 19–98.

Tropper, P., Manning, C., 2007. The solubility of corundum in H_2O at high pressure and temperature and its implications for Al mobility in the deep crust and upper mantle. Chem. Geol. 240, 54–60.

Tsay, A., Zajacz, Z., Sanchez-Valle, C., 2014. Efficient mobilization and fractionation of rare-earth elements by aqueous fluids upon slab dehydration. Earth Planet. Sci. Lett. 398, 101–112.

Wang, P., Anderko, A., 2001. Computation of dielectric constants of solvent mixtures and electrolyte solutions. Fluid Phase Equilib. 186 (1), 103–122.

Walther, J.V., 1992. Ionic association in H_2O–CO_2 fluids at mid-crustal conditions. J. Metamorph. Geol. 10, 789–797.

Walther, J.V., Helgeson, H.C., 1980. Description and interpretation of metasomatic phase relations at high pressures and temperatures. 1. Equilibrium activities of ionic species in nonideal mixtures of CO_2 and H_2O. Am. J. Sci. 280, 575–606.

Walther, J.V., Schott, J., 1988. The dielectric constant approach to speciation and ion pairing at high temperature and pressure. Nature, 635–638.

Wen, D., Olesik, S.V., 2000. Characterization of pH in liquid mixtures of methanol/H_2O/CO_2. Anal. Chem. 72, 475–480.

Widmer, T., Thompson, A.B., 2001. Local origin of high pressure vein material in eclogite facies rocks of the Zermatt-Saas Zone, Switzerland. Am. J. Sci. 301 (7), 627–656.

Wohlers, A., Manning, C.E., 2009. Solubilityof corundum in aqueous KOH solutions at 700 °C and 1 GPa. Chem. Geol. 262, 310–317.

Wohlers, A., Manning, C.E., Thompson, A.B., 2011. Experimental investigation of the solubility of albite and jadeite in H_2O, with paragonite + quartz at 500 and 600 °C, and 1–2.25 GPa. Geochim. Cosmochim. Acta 75, 2924–2939.

Wolery, T.J., 1992. EQ3/6: A software package for geochemical modeling of aqueous systems: package overview and installation guide (version 7.0). Lawrence Livermore National Laboratory, Livermore, CA.

Yardley, B.W.D., Graham, J.T., 2002. The origins of salinity in metamorphic fluids. Geofluids 2, 249–256.

Yoshii, N., Miura, S., Okazaki, S., 2001. A molecular dynamics study of dielectric constant of water from ambient to sub- and supercritical conditions using a fluctuating-charge potential model. Chem. Phys. Lett. 345 (1), 195–200.

Zhang, Z., Duan, Z., 2005. Prediction of the *PVT* properties of water over wide range of temperatures and pressures from molecular dynamics simulation. Phys. Earth Planet. Inter. 149, 335–354.

Zotov, N., Keppler, H., 2000. In-situ Raman spectra of dissolved silica species in aqueous fluids to 900 °C and 14 kbar. Am. Mineral. 85, 600–604.